

In vivo and *in vitro* tracking of erosion in biodegradable materials using non-invasive fluorescence imaging

Natalie Artzi^{1,2*}, Nuria Oliva^{1,3}, Cristina Puron^{1,3}, Sagi Shitreet^{1,4}, Shay Artzi⁵, Adriana bon Ramos^{1,3}, Adam Groothuis⁶, Gary Sahagian⁷ and Elazer R. Edelman^{1,8}

The design of erodible biomaterials relies on the ability to program the *in vivo* retention time, which necessitates real-time monitoring of erosion. However, *in vivo* performance cannot always be predicted by traditional determination of *in vitro* erosion^{1,2}, and standard methods sacrifice samples or animals³, preventing sequential measures of the same specimen. We harnessed non-invasive fluorescence imaging to sequentially follow *in vivo* material-mass loss to model the degradation of materials hydrolytically (PEG:dextran hydrogel) and enzymatically (collagen). Hydrogel erosion rates *in vivo* and *in vitro* correlated, enabling the prediction of *in vivo* erosion of new material formulations from *in vitro* data. Collagen *in vitro* erosion was used to infer physiologic *in vitro* conditions that mimic erosive *in vivo* environments. This approach enables rapid *in vitro* screening of materials, and can be extended to simultaneously determine drug release and material erosion from a drug-eluting scaffold, or cell viability and material fate in tissue-engineering formulations.

Biodegradable materials serve as platforms for structural stabilization, void filling, drug delivery and tissue engineering^{4–8}, offering the promise of reduced complications posed by permanent foreign objects⁹. However, controlled material development is limited, as degradation *in vivo* is more complex than *in vitro*, and *in vitro* assays are rarely adequate measures of implant behaviour. Loss of material integrity, structure, and eventually mass, progress dependently over time but are dominated by different environmental forces *in vitro* and *in vivo*. The question remains as to whether erosion or loss of mass in one domain can predict performance in the other. Gravimetric determinations from periodic sampling of explant weight cannot follow the same formulation over time, necessitate a large number of animals to follow a small number of samples, and have excessive variability^{3,10–13}. Chromatography tracks molecular weight changes^{2,12} but cannot be applied to eliminable materials that do not undergo chain scission. Material environment affects erosion, and the material and degradation products may affect the environment in turn^{14,15}. Thus, *in vivo* residence times and *in vitro* durability of three-dimensional degradable structures differ².

We developed a non-invasive imaging technique that tracks material erosion *in vivo* through a fluorescent tag covalently

attached to components of model materials. Materials erosion was calculated from the decay in total material fluorescence signal using non-invasive *In Vivo* Imaging System (IVIS). Model hydrolytically degradable adhesive materials used herein are based on polyethylene glycol (PEG) amine and dextran aldehyde^{16,17}. PEG replete with amine groups and oxidized dextran react at body temperature in a Schiff base reaction to form adhesive materials as aldehydes bind to tissue amines. The reaction is reversible and the material hydrolyzes to its polymeric components^{16,17}. Although PEG polymers may undergo enzymatic degradation, significant fluid uptake and swelling dominate the degradation of our formulated PEG:dextran hydrogels, resulting in hydrolytically sensitive materials. As material shape dictates fluid uptake, we examined whether fluorescence tracking could distinguish the fate of PEG:dextran formulations cast in a series of shapes, sizes and varying PEG solid content. Compressed denatured type II collagen was used as a model for an enzymatically degradable material, the erosion profile of which should change with implantation site and natural variation in enzyme content.

To enable the use of tagged materials to measure erosion rate, we verified that fluorescent tagging had no effect on material properties. Indeed, the swelling and erosion kinetics (Supplementary Fig. S1a), gelation time (Supplementary Fig. S1b) and adhesion to biological tissues (Supplementary Fig. S1c) of PEG:dextran were unaffected by 5% fluorescent PEG (demonstrated using the following formulation of dextran, D10-50-14, and PEG, P8-10-40, as described in Supplementary Table S2). Fluorescent tag tracking, however, provides different erosion kinetics from conventional wet gravimetric analysis. The two assays demonstrated an identical duration of material integrity. However, whereas tag-tracking indicated immediate erosion on immersion, gravimetric determinations indicated a gain in material weight until swelling peaked (Supplementary Fig. S2). Indeed, erosion determined by gravimetric analysis was 40% faster than by fluorescent tracking, as the former probably considers elution of media trapped within the network during swelling and not just erosion of polymeric chains. When the effect of swelling was eliminated and gravimetric analysis was performed after samples were dried, the erosion profile coincided with the fluorescent profile (Supplementary Fig. S2), up to the limit of

¹Harvard-MIT Division of Health Sciences and Technology, Massachusetts Institute of Technology, E25-449, 77 Massachusetts Ave., Cambridge, Massachusetts 02139, USA, ²Department of Anesthesiology, Brigham and Women's Hospital, Harvard Medical School, Boston, Massachusetts 02115, USA, ³Institut Quimic de Sarrià, Universitat Ramon Llull, Barcelona, 08017, Spain, ⁴Ort Braude College, Karmiel 21982, Israel, ⁵IBM Research, Hawthorne, New York 10532, USA, ⁶Concord Biomedical Sciences and Emerging Technologies, Lexington, Massachusetts 02421, USA, ⁷Department of Physiology, Tufts University School of Medicine, Boston, Massachusetts 02111, USA, ⁸Cardiovascular Division, Department of Medicine, Brigham and Women's Hospital, Harvard Medical School, Boston, Massachusetts 02115, USA. *e-mail: nartzi@mit.edu.

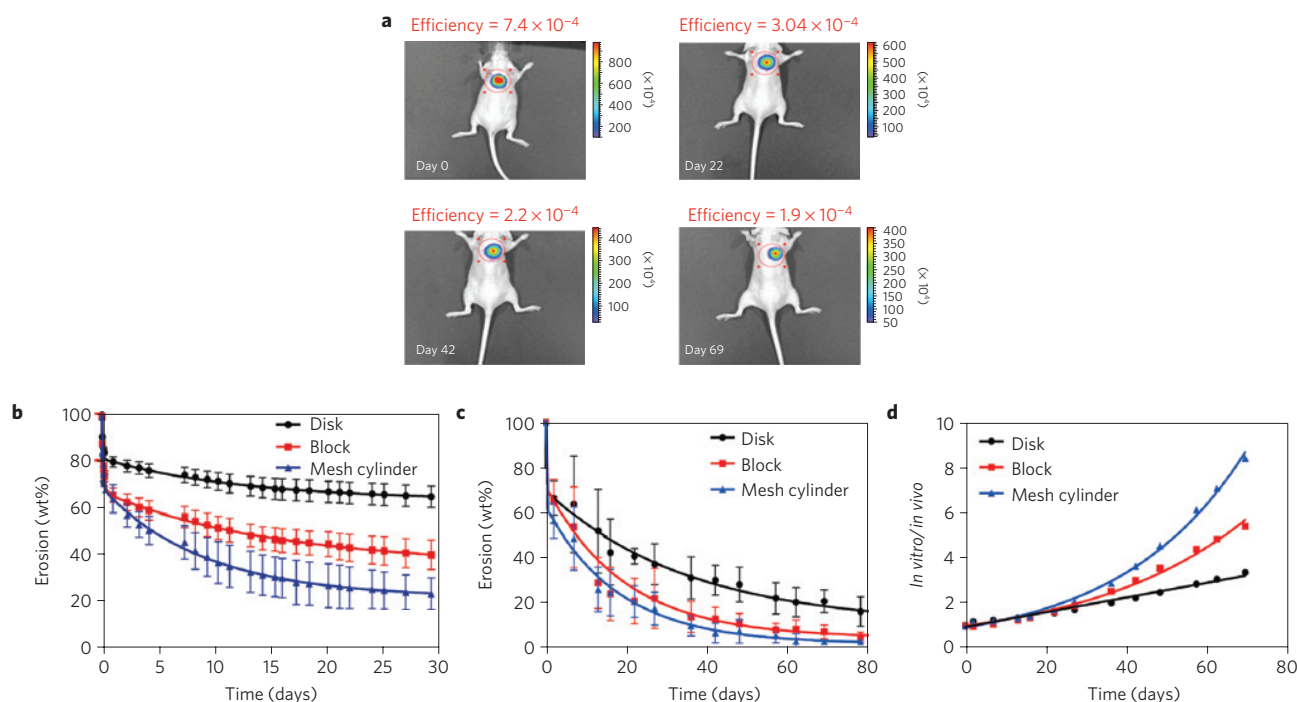


Figure 1 | *In vitro*-*in vivo* erosion profiles of PEG:dextran correlate and vary with material surface area. *In vitro* and *in vivo* erosion profiles of PEG:dextran (D10-50-14 P8-10-40) cast in a series of shapes are depicted by tracking the loss of fluorescence intensity with time. **a**, The effect of material shape on degradation profile was followed *in vivo* non-invasively in the dorsal subcutaneous space of mice (disk shaped materials are presented). **b-d**, The loss of fluorescence signal with time *in vitro* (**b**) and *in vivo* (**c**) was converted to weight loss and correlated (**d**). An excellent correlation was found between mean values of *in vitro* and *in vivo* erosions of disks $\ln\text{-}in\text{-}vivo_{\text{disk}} = 0.033t + 0.93$; ($R = 0.96$), block $\ln\text{-}in\text{-}vivo_{\text{block}} = 0.928 \cdot \exp(0.27 \cdot t)$; ($R = 0.94$) and mesh cylinders $\ln\text{-}in\text{-}vivo_{\text{mesh}} = 0.934 \cdot \exp(0.032 \cdot t)$; ($R = 0.98$). Disk erosion *in vivo* tracked linearly with erosion *in vitro* (**d**, $R = 0.98$). Thin blocks and mesh cylinders with significantly higher surface area than the disks (116, 190 and 86 mm² respectively) showed accelerated erosion *in vitro* compared with the erosion *in vivo*, leading to an exponential dependence of the ratio between *in vivo* and *in vitro* erosion with time (**d**, $R = 0.99$ for both shapes).

scale sensitivity in the regime where fluorescent quantification remains constantly sensitive. Such drying removes samples from further experimentation and is inappropriate for *in vivo* implants. Fluorescent tracking allows high fidelity identification of polymeric chains released from the bulk gel sequentially from the onset of immersion and without sample destruction.

Hydrophilic material swelling and dissolution is determined by fluid uptake, which is modulated by the material surface area and volume of diluent⁴. We examined material loss profiles in both domains for disks, blocks or hollow mesh cylinders of PEG:dextran (D10-50-14 P8-10-40, Supplementary Fig. S3) all containing 5% fluorescent PEG with fixed mass. Construct erosion *in vivo* was calculated from efficiency signals in the region of interest around the sample (Fig. 1a). Erosion was biphasic—comprised of rapid sample loss, presumably through diffusion of non-crosslinked, unreacted PEG and dextran polymeric chains, followed by more gradual degradation of the crosslinked copolymer network. In each case, erosion kinetics *in vivo* was faster, but tracked with the biphasic behaviour seen *in vitro* (Fig. 1b–c). Thin blocks and mesh cylinders with significantly higher surface area than the disks showed, not unexpectedly, accelerated erosion *in vitro* compared with the erosion *in vivo*, leading to an exponential dependence of the ratio between *in vivo* and *in vitro* erosion with time (Fig. 1d, $R = 0.99$ for both shapes). In contrast, disk erosion was limited by diluent volume, and in fixed volume environments *in vivo* erosion kinetics tracked linearly with erosion *in vitro* (Fig. 1d, $R = 0.98$).

Within each hydrogel shape, formulation protocols control erosion profiles, as network formation dictates fluid uptake and depends on the aldehyde:amine ratio. As this ratio is determined by the relative amounts of PEG and dextran, we examined the

effect of PEG solid content on erosion over a range limited by PEG solubility (Fig. 2a). At solid content less than 10 wt%, constructs lose structural integrity; at higher solid content, better stability is observed to a threshold value (above 20 wt%). Each data set adhered to the expected erosion profile and fit a dual exponential decay model. In this model, polymer mass, M , follows the erosion of two components—free (M_1) and crosslinked (M_2) material—each defined by the relative proportion of total mass, and a specific erosive rate constant, k , at each phase $M = M_1 \cdot e^{(-k_1 t)} + M_2 \cdot e^{(-k_2 t)}$.

The relative measures of the mass components provide an indirect determination of gel content and degree of crosslinking. Although the ratio of unbound and bound rate constants (k_1/k_2) spans an order of magnitude with changes in shape, in a fascinating manner the relationship between *in vivo* and *in vitro* ratios is virtually fixed at 2 (Supplementary Table S1), providing a valuable means of assessing erosion in this system. The relative rates of erosion of crosslinked and free material might allow one to infer *in vivo* behaviour from *in vitro* performance, and the very acceleration of *in vitro* erosion can be used to predict *in vivo* erosion. As the number of amine groups increases with PEG content, the unbound component drops exponentially (Fig. 2c), but overall erosion is still determined by the rate constant of the bound or crosslinked phase rate (k_2) (Fig. 2b). Erosion is limited by crosslinking, and as the number of amine groups available for gel formation rises, erosion rate drops significantly.

We validated this bi-exponential erosion model and model predictability by prospectively predicting adhesive erosion profiles for newly synthesized PEG:dextran formulations with 10 or 14% PEG solid contents (formulations specified in Supplementary Table S2). Erosive behaviour was calculated using values for

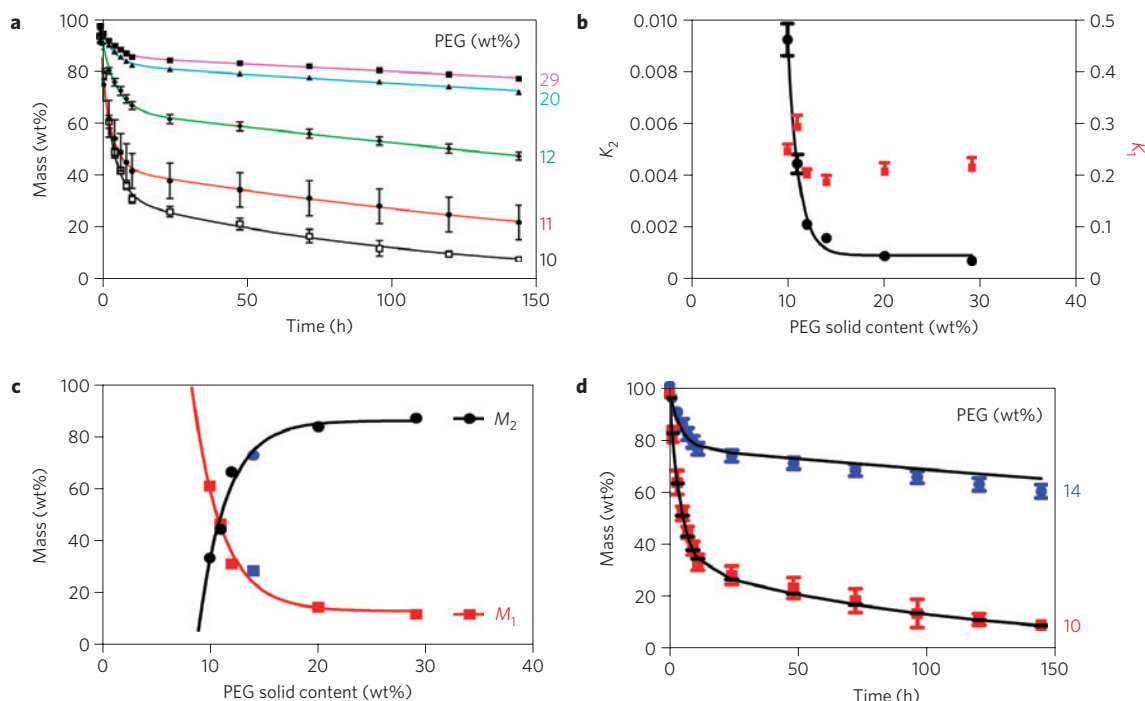


Figure 2 | Dual exponential decay model describes PEG:dextran *in vitro* erosion and enables the prospective prediction of the erosion profile of new material formulations. **a**, Alteration of PEG solid content from 10 to 29 wt% enables fine-tuning of material erosion kinetics. Model descriptors are presented as a function of PEG solid content. **b,c**, Whereas k_1 is constant and k_2 decays exponentially (**b**), M_1 and M_2 similarly demonstrate reciprocal exponential changes with PEG solid content (**c**). The relationships between model descriptors and PEG solid content (PEG_{SC}) are as follows: $k_2 = 53.7 \cdot \exp(-0.88 \cdot (\text{PEG}_{\text{SC}})) + 0.0009$, $M_1 = 3,979 \cdot \exp(-0.44 \cdot (\text{PEG}_{\text{SC}})) + 12.4$ and $M_2 = -3,028 \cdot (1 - \exp(-0.41 \cdot (\text{PEG}_{\text{SC}}))) + 85.4$. **d**, Using the equations describing the relation between model descriptors and PEG solid content, the erosion profile of new compositions containing 10 and 14 wt% PEG were prospectively predicted (points are empirically accumulated and lines are model predictions). Constants were extrapolated from the data fits and are inserted in the figures as blue symbols; squares represent k_1 and M_1 and circles represent k_2 and M_2 . Predicted erosion correlated well with empirical observations (Pearson's coefficient $R = 0.99$).

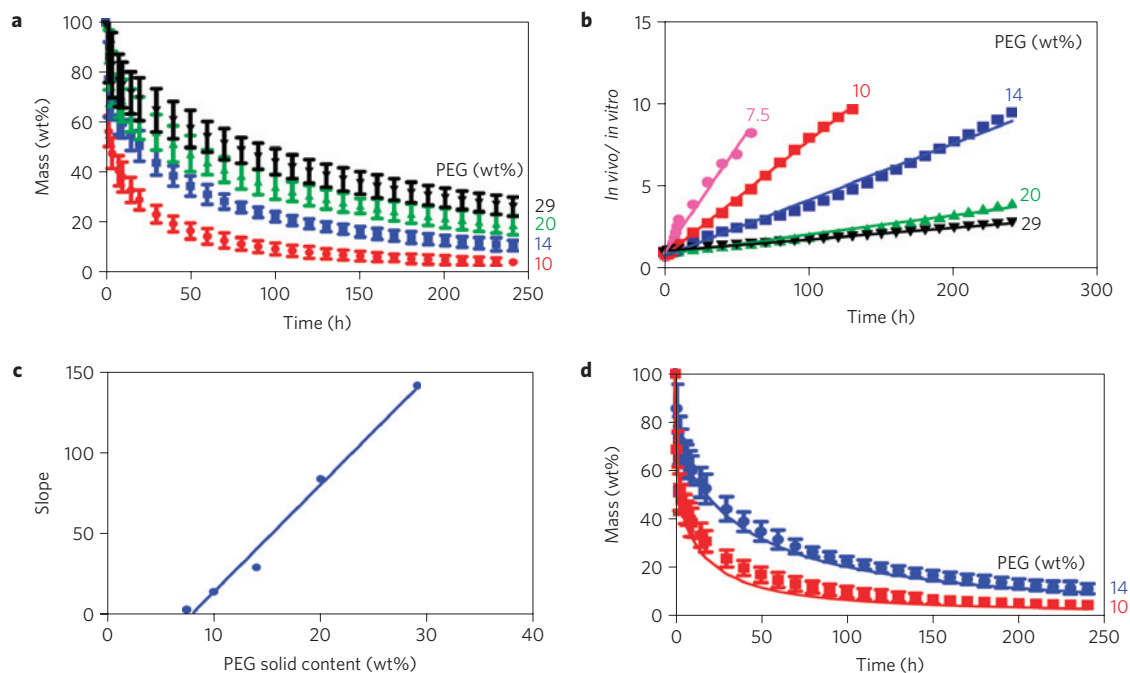


Figure 3 | *In vitro-in vivo* correlation of PEG:dextran erosion profiles enables prediction of *in vivo* erosion kinetics from *in vitro* data. **a**, *In vivo* erosion of PEG-dextran formulations is depicted and follows the trend of the *in vitro* erosion profile, at a faster pace, as demonstrated for compositions with 10, 14, 20 or 29 wt% PEG solid content. **b**, A linear relationship exists between the ratio of *in vivo* and *in vitro* erosion as a function of time for all PEG solid contents examined. **c**, The slopes of these curves linearly correlate with PEG solid content. **d**, Using this linear relationship, *in vivo* erosion profiles of two different formulations were accurately predicted from *in vitro* data ($R = 0.99$) (points are empirically accumulated and lines are model predictions).

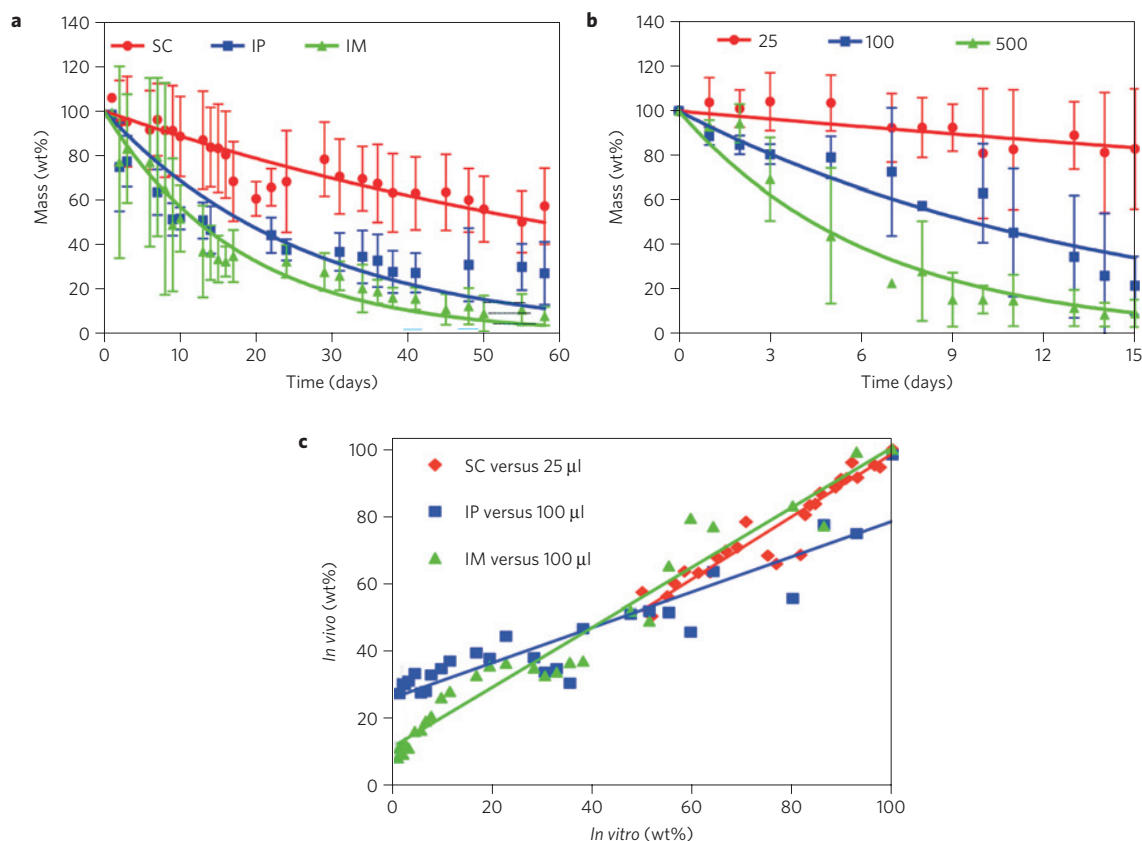


Figure 4 | *In vivo* erosion profile is site-dependant and can be used to infer physiologically relevant *in vitro* conditions for enzymatic materials. *In vitro* and *in vivo* erosion of compressed denatured type II collagen are presented. **a**, *In vivo* erosion at target sites that differ in enzyme concentration and fluid volume (Subcutaneous (SC), intraperitoneal (IP) and intramuscular (IM)) is site dependent and fits one exponential decay model ($R = 0.44$, 0.77 , and 0.7 for SC, IP and IM). The *in vivo* erosion profiles were used to infer physiologically relevant conditions of diluent volume and enzyme concentration.

b,c, Although *in vitro* erosion depends both on enzyme concentration and fluid volume, a specific set of conditions resulted in an *in vitro* erosion profile ($R = 0.71$, 0.9 , and 0.95 for SC, IP and IM) (**b**) that linearly correlates with the *in vivo* erosion (**c**). The erosion in both domains fits an exponential decay model. A correlation between the erosion profiles *in vitro* and *in vivo* is achieved when SC implantation is plotted versus *in vitro* erosion of material submerged in $25\ \mu\text{l}$ of PBS solution containing physiological concentration of collagenase, and for IM and IP implantations when compared with *in vitro* erosion using $100\ \mu\text{l}$ of PBS-containing enzyme solution. The linear correlation between *in vitro* and *in vivo* erosion enables screening of materials *in vitro* with *in vivo* prediction capacity.

M_1 , M_2 , k_1 and k_2 extracted from the fits of data in Fig. 2b,c, and correlated exceptionally well with empirical measures of erosion (Fig. 2d, $R = 0.99$).

The greatest benefit of such a model would be the ability to predict *in vivo* erosion kinetics of newly synthesized materials from *in vitro* data. This would minimize the number of animals used and also serve as a convenient screening platform *in vitro*. Interestingly, *in vivo* erosion (Fig. 3a) followed the expected exponential decay and differed with PEG solid content material erosion, as seen with disks *in vitro* (Fig. 2a), establishing a fixed linear relationship between the *in vitro* and *in vivo* erosion versus time for all formulations (Fig. 3b). The ratio of erosion rates in both domains correlates with PEG solid content (Fig. 3c). This highly sensitive correlation was used to accurately predict *in vivo* performance based on *in vitro* data for all samples in this formulation type (Fig. 3d, $R = 0.99$). Successful prediction of material erosion demonstrates continuity within the design space and the potential for strategic adjustment of the PEG:dextran composition to meet specific requirements.

PEG:dextran mixtures are dominated by hydrolytic erosive forces; other materials are subject to a more complex array of forces, which often cannot be reproduced and the impact of which is impossible to intuit. Fluorescent tracking enables us to assume that correlation will exist for a specific environmental condition

set and, once attained, to infer that these are the physiologic values. We examined compressed collagen matrices, materials increasingly used in tissue engineering applications and the degradation of which requires fluid imbibition, material swelling, enzyme penetration and enzymatic bulk degradation (Fig. 4). As with hydrogels, the volume of diluent fluid is critical for erosion, but is increasingly complex in the case of enzymatic degradation. Diffusion of enzymes into samples and of degradation products out of samples requires swelling. Hence, the surrounding fluid volume determining the degree of swelling should be considered in addition to the classic Michaelis–Menten enzyme kinetics¹⁸. Swelling of our collagen-based material is significantly affected by diluent volume with identical enzyme concentration (Supplementary Fig. S4). Whereas the subcutaneous space of a mouse has a limited fluid volume, the intraperitoneal cavity is significantly larger, with higher volume of fluids. Thus, not unexpectedly, erosion kinetics *in vitro* correlated best with *in vivo* behaviour for specific immersion volumes that varied with implant site (Fig. 4). *In vitro* erosion under $25\ \mu\text{l}$ diluent correlated very well with *in vivo* erosion in the subcutaneous space. A linear relationship was obtained for intramuscular and intraperitoneal erosions when $100\ \mu\text{l}$ diluent volume was used *in vitro*. In a most intriguing manner the inferred volumes and concentration align remarkably with empirically obtained values reported in the literature¹⁹.

As with the hydrogels, gravimetric analysis of collagen matrices underestimated erosion early and overestimated erosion late. Sample drying shifted these measures to coincide with fluorescent assays, once again verifying the contamination of signal with swelling. The gravimetric analysis, however, was further limited, as increasingly sensitive scales would be needed to track sample weight changes in the regime where fluorescent quantification remains sensitive (Supplementary Fig. S5).

Tracking material erosion is challenging. *In vivo* performance rarely coincides with erosion *in vitro*. Material fate varies with material dimensions, crosslinking and composition, and environmental conditions and stresses *in vitro* that do not necessarily represent the *in vivo* state. Pathophysiological conditions such as inflammation cannot be recapitulated *in vitro*. Two questions arise—will erosion *in vivo* follow erosion *in vitro* even if they occur at different rates? And, if there is a match between performances in the two domains, can one be predicted from the other? Indeed, one could use *in vitro* behaviour as a surrogate for erosion *in vivo* if such a correlation exists. Here we report that intravital tracking of fluorescent tags on degradable materials can be used similarly *in vivo* and *in vitro*, with a minimum of samples, sequentially on the same specimen, with significant accuracy and, most importantly, in a correlative fashion. *In vivo* erosion of our selected materials, which degrade primarily by hydrolytic or enzymatic degradation, correlates with *in vitro* erosion, allowing prediction of the former from the latter. Moreover, erosive materials can be considered as scaffold-tethered drugs²⁰, where erosion kinetics as being similar to release kinetics can be successfully modelled with a dual exponent system with free and crosslinked polymer elements comparable to free and bound drug (Fig. 1). Such a system can also now explain the impact of material shape and dimensions, and material formulation protocols on erosion profiles (Figs 2–3), facilitating the design of materials with programmed retention time. Equally important is that such a system gives a great insight into the mechanism of erosion and the physiological conditions that need to be established *in vitro* to attain correlation. We can now explain how and why materials implanted in different target sites, including the subcutaneous, intramuscular and intraperitoneal spaces, resulted in distinctive erosion profiles. Although enzymatic degradation of materials *in vivo* is very complex, under the specific set of conditions we have been using, collagen-based material degradation *in vivo* could be recapitulated *in vitro* by variation in fluid volume with physiological enzyme concentrations (Fig. 4a). It is remarkable how the definition of the *in vivo* conditions leads to a linear correlation between *in vivo* and *in vitro* erosion profiles (Fig. 4b–c).

The ability to detect and predict the time course of *in vivo* erosion is crucial to the design, informed regulation and use of the increasing number of biomedical devices with erosive properties. Although the data published in this manuscript are material- and conditions-specific, our approach can be adapted to track the erosion of multiple material systems. Moreover, erosion tracking can be extended beyond the hydrolytic and enzymatic processes examined here to include complex conjugations. Use of multiple tags can enable examination of material dynamics, and even the interaction between molecules using advanced fluorescent methods, such as Fluorescent Resonance Energy Transfer (FRET). The incorporation of multiple concomitant tags allows independent tracking and correlation of drug release and material loss from a polymer drug-eluting scaffold^{21–23}, or the fate of cells and materials within tissue-engineered formulations^{24,25}. When tagging is not possible, one could entrap fluorescent molecules, for example quantum dots, that would serve as surrogates for erosion. It is now possible to follow the fate of erosive materials in a precise and reproducible manner that can be used *in vivo* and *in vitro* and is amenable to mathematical modelling and prospective prediction.

Methods

Quantifying material erosion using fluorescent signal *ex vivo*. Mass loss kinetics, as measured by gravimetric analysis, was compared with erosion profiles obtained by following the fluorescent signal loss of labelled materials. To enable erosion detection via optical imaging, PEG was labelled with fluorescein, and collagen with Texas Red.

Fluorescein-labelled PEG was synthesized as follows: 2.4 g PEG amine was dissolved in 6 ml dichloromethane. Fluorescein-5-carboxyamido hexanoic acid (Invitrogen) was added to the solution, followed by addition of 12 μ l triethylamine (Sigma). The mixture was stirred at room temperature for 48 h. The solid that remained after solvent evaporation was dissolved in 100 ml double distilled water, dialyzed and lyophilized. PEG solution containing 1% fluorescent PEG was mixed with dextran aldehyde to prepare fluorescent gels. While materials were submerged in 2 ml PBS and shaken at 37 °C, media were exchanged daily and the fluorescence intensity in the media was measured using an excitation wavelength of 485 nm and emission wavelength of 538 nm. The erosion profile was followed by quantifying the loss of fluorescent signal with time.

Texas Red-labelled collagen was synthesized by reacting the collagen sponges with Texas Red-T succinimidyl ester (5.6 μ l per sponge) in 0.2 M bicarbonate buffer (0.320 ml per sponge), for 2 h at room temperature. The sponges were rinsed three times in PBS to remove excess unreactive dye.

Stability of PEG-fluorescein bond. To verify that the fluorescent tag remains attached to the polymer materials, 1 ml PEG-F* was placed in a dialysis membrane of cellulose ester (Spectra/Por Biotech, MWCO = 1,000, #131096) surrounded by 100 ml PBS 1 \times . Free fluorescein could then diffuse out, and the media was scanned intermittently using excitation and emission wavelengths of 485 and 538 nm, respectively, to quantify the amount of free and detached tag with time.

Quantifying material erosion using fluorescent signal *in vivo*. Sterile solutions passed through 0.2 mm filters were used to prepare PEG:dextran constructs in the shapes of disks, blocks and coated mesh cylinders of the same dimensions as used for *in vitro* evaluation. The constructs were implanted subcutaneously in isoflurane-anaesthetized nude albino mice (Charles River Labs) through a 1 cm skin incision into the dorsal subcutaneous space of the mice. The incision and pocket were closed with 7–0 prolene sutures.

Sterile collagen-based samples, 4 mm in diameter, were similarly implanted into the subcutaneous space of mice (SC), intraperitoneally (IP) and intramuscularly (IM). Immediately, and at various intervals after surgery, the animals were imaged using the Xenogen IVIS device with the appropriate filter sets. The fluorescence intensity was determined by calculating the efficiency overlying each construct, where the fluorescence intensity is corrected to eliminate tissue autofluorescence. Whereas fluorescein was used for SC implantations, Texas Red was used for deeper target sites (IM and IP) to avoid photo bleaching and light penetration issues. The choice of fluorescent dye is critical, especially when tracking materials for extended period of times. Optimal dyes are near-infrared dyes that do not undergo photobleaching during the experimental period or overlap with tissue autofluorescence.

Statistical analyses. Data are presented as mean \pm standard deviation unless otherwise indicated ($n = 3$ for *in vitro* swelling and degradation, adhesion and gelation time of PEG:dextran formulations, $n = 5$ for *in vitro* erosion characterization of collagen-based samples, $n = 5$ and 10 for *in vivo* erosion tracking of PEG:dextran and collagen-based formulations, respectively). To take multiple comparisons into account, when comparing swelling and degradation, statistical comparisons were done using two way ANOVA with replication. A P -value < 0.05 was considered to denote statistical significance.

Received 11 March 2011; accepted 11 July 2011; published online 21 August 2011; corrected after print 20 September 2011

References

1. Bruggeman, J. P., de Bruin, B. J., Bettinger, C. J. & Langer, R. Biodegradable poly(polyol sebacate) polymers. *Biomaterials* **29**, 4726–4735 (2008).
2. Grayson, A. C. *et al.* Differential degradation rates *in vivo* and *in vitro* of biocompatible poly(lactic acid) and poly(glycolic acid) homo- and co-polymers for a polymeric drug-delivery microchip. *J. Biomater. Sci.* **15**, 1281–1304 (2004).
3. Benny, O. *et al.* *In vivo* fate and therapeutic efficacy of PF-4/CTF microspheres in an orthotopic human glioblastoma model. *FASEB J.* **22**, 488–499 (2008).
4. Gopferich, A. Mechanisms of polymer degradation and erosion. *Biomaterials* **17**, 103–114 (1996).
5. Anseth, K. S., Shastri, V. R. & Langer, R. Photopolymerizable degradable poly(hydroxyacrylates) with osteocompatibility. *Nature Biotechnol.* **17**, 156–159 (1999).
6. Falco, E. E., Patel, M. & Fisher, J. P. Recent developments in cyclic acetal biomaterials for tissue engineering applications. *Pharm. Res.* **25**, 2348–2356 (2008).
7. Lee, H. *et al.* Local delivery of basic fibroblast growth factor increases both angiogenesis and engraftment of hepatocytes in tissue-engineered polymer devices. *Transplantation* **73**, 1589–1593 (2002).

8. Little, S. R. *et al.* Poly- β amino ester-containing microparticles enhance the activity of nonviral genetic vaccines. *Proc. Natl Acad. Sci. USA* **101**, 9534–9539 (2004).
9. Ifkovits, J. L. & Burdick, J. A. Review: Photopolymerizable and degradable biomaterials for tissue engineering applications. *Tissue Eng.* **13**, 2369–2385 (2007).
10. Mahdavi, A. *et al.* A biodegradable and biocompatible gecko-inspired tissue adhesive. *Proc. Natl Acad. Sci. USA* **105**, 2307–2312 (2008).
11. Bettinger, C. J., Bruggeman, J. P., Borenstein, J. T. & Langer, R. S. Amino alcohol-based degradable poly(ester amide) elastomers. *Biomaterials* **29**, 2315–2325 (2008).
12. Witt, C., Mader, K. & Kissel, T. The degradation, swelling and erosion properties of biodegradable implants prepared by extrusion or compression moulding of poly(lactide-co-glycolide) and ABA triblock copolymers. *Biomaterials* **21**, 931–938 (2000).
13. Kim, J. *et al.* Synthesis and evaluation of novel biodegradable hydrogels based on poly(ethylene glycol) and sebacic acid as tissue engineering scaffolds. *Biomacromolecules* **9**, 149–157 (2008).
14. Chao, G. T. *et al.* Synthesis, characterization, and hydrolytic degradation behavior of a novel biodegradable pH-sensitive hydrogel based on polycaprolactone, methacrylic acid, and poly(ethylene glycol). *J. Biomed. Mater. Res.* **85**, 36–46 (2008).
15. Kost, J., Leong, K. & Langer, R. Ultrasound-enhanced polymer degradation and release of incorporated substances. *Proc. Natl Acad. Sci. USA* **86**, 7663–7666 (1989).
16. Artzi, N. *et al.* Characterization of star adhesive sealants based on PEG/Dextran hydrogels. *Macromol. Biosci.* **9**, 754–765 (2009).
17. Artzi, N., Shazly, T., Baker, A. B., Bon, A. & Edelman, E. R. Aldehyde-amine chemistry enables modulated biosealants with tissue-specific adhesion. *Adv. Mater.* **21**, 3399–3403 (2009).
18. Tzafriri, A. R., Bercovier, M. & Parnas, H. Reaction diffusion model of the enzymatic erosion of insoluble fibrillar matrices. *Biophys. J.* **83**, 776–793 (2002).
19. Hartveit, F. & Thunold, S. Peritoneal fluid volume and the oestrus cycle in mice. *Nature* **210**, 1123–1125 (1966).
20. Tzafriri, A. R. Mathematical modeling of diffusion-mediated release from bulk degrading matrices. *J. Control Release* **63**, 69–79 (2000).
21. Shi, X. *et al.* Novel mesoporous silica-based antibiotic releasing scaffold for bone repair. *Acta Biomater.* **5**, 1697–1707 (2009).
22. Zhang, C. *et al.* Loading dependent swelling and release properties of novel biodegradable, elastic and environmental stimuli-sensitive polyurethanes. *J. Control Release* **131**, 128–136 (2008).
23. Nuttelman, C. R., Tripodi, M. C. & Anseth, K. S. Dexamethasone-functionalized gels induce osteogenic differentiation of encapsulated hMSCs. *J. Biomed. Mater. Res.* **76**, 183–195 (2006).
24. Riboldi, S. A., Sampaolesi, M., Neuenschwander, P., Cossu, G. & Mantero, S. Electrospun degradable polyesterurethane membranes: Potential scaffolds for skeletal muscle tissue engineering. *Biomaterials* **26**, 4606–4615 (2005).
25. Levenberg, S. *et al.* Engineering vascularized skeletal muscle tissue. *Nature Biotechnol.* **23**, 879–884 (2005).

Acknowledgements

The authors acknowledge the NIH (GM/HL 49039, UL1 RR 025758 to ERE) and the MIT Deshpande Centre for the financial support of this work. We would like to thank R. Tzafriri for discussions and suggestions on modelling. We thank J. Karp, E. Levine and M. Carcole for assisting in the preparation of the manuscript.

Author contributions

N.A. conceived the ideas, designed and directed the research. N.A., N.O., C.P., S.S., A.G. and A.b.R. conducted the experiments. N.A. and S.A. performed the mathematical modelling. G.S. contributed reagents and technical expertise. E.R.E. participated in the data analysis and model synthesis. N.A. and E.R.E. wrote the manuscript.

Additional information

The authors declare no competing financial interests. Supplementary information accompanies this paper on www.nature.com/naturematerials. Reprints and permissions information is available online at <http://www.nature.com/reprints>. Correspondence and requests for materials should be addressed to N.A.

ERRATUM

***In vivo* and *in vitro* tracking of erosion in biodegradable materials using non-invasive fluorescence imaging**

Natalie Artzi, Nuria Oliva, Cristina Puron, Sagi Shitreet, Shay Artzi, Adriana bon Ramos, Adam Groothuis, Gary Sahagian and Elazer R. Edelman

Nature Materials **10**, 704–709 (2011); published online 21 August 2011; corrected after print 20 September 2011.

In the version of this Letter originally published, the *x*-axis units of Fig. 4a and b should have been days instead of hours. This error has been corrected in the HTML and PDF versions of the Letter.